AST2210 - Exercise 1

Candidate number: 15624
(Dated: October 18, 2024)

Using observational data from the Swedish 1-m Solar Telescope we can visualize how mass in the solar photosphere moves. This is visualized for a rectangular field of view with size a little smaller than the surface area of the Earth. By fitting a Gaussian function to the spectra for each pixel location in our field of view we calculate the Doppler velocities in the whole grid and make a Doppler map. Comparing this Doppler map to an intensity image we see that the light from granule centers are blueshifted as this is gas moving towards us from the surface, while the light from intergranular lanes appear redshifted as the gas is moving away from us.

I. INTRODUCTION

Studying the intensity from the solar surface can tell us many things. From studying absorption spectra of the Sun, we can calculate the Doppler velocities of moving mass and find out if the mass is bursting from the surface or retracting. In this report we will study observational data taken by the Swedish 1-m Solar Telescope on La Palma to study the motion of material in the solar photosphere. First we will study the absorption spectra for different locations in a rectangular field of view on the surface, then we will plot an intensity image of the same field of view to study the granulation pattern, and lastly we will calculate the Doppler velocities to make a Doppler map that shows us how the surface mass is moving.

II. THEORY

There are different kinds of instruments one can use for solar observations. One instrument frequently used is a Fabry-Pérot interferometer, but a slit spectrograph is also possible to use.

A. Slit-spectrograph

A slit-spectrograph is an instrument used for spectroscopy. The instrument works by first letting light through a small slit as shown in figure 1 to adjust the amount of light entering the spectrograph. Then a grating is typically used to disperse the light, separating it into different wavelengths [1]. We can explain what happens in the grating by first looking at what happens when light passes through a single slit. When light passes through a narrow single slit, it diffracts, creating an interference pattern of brighter and darker regions on the screen or detector placed on the opposite side of the slit. The brightest regions is where the light constructively interfere. Longer wavelengths will diffract more, resulting in the brighter regions appearing closer together than for shorter wavelengths. A grating consists of multiple slits placed side by side. Increasing the number of slits results in a more defined interference pattern with higher intensity. The slit-spectrograph is used in solar physics to split light into specific wavelengths as shown in figure 2 and studying their spectra [2].

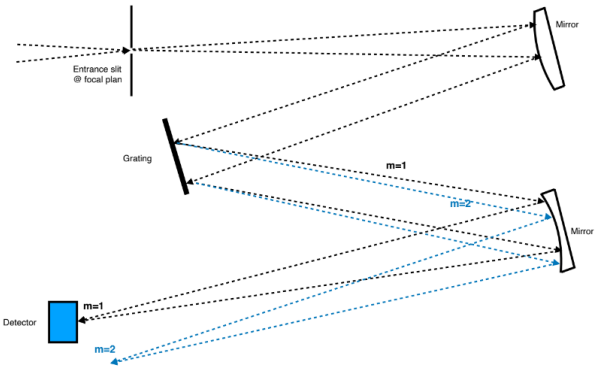

Figure 1: The set up of a slit-spectrograph with a diffraction grating [3].

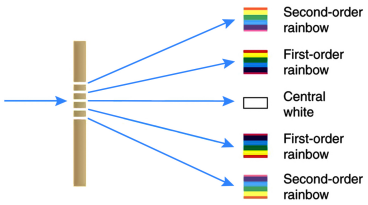

Figure 2: Diffraction pattern created by multiple slits like we have in a grating [4].

B. Fabry-Pérot interferometer

The Fabry-Pérot interferometer can also be used for spectroscopy. As shown in figure 3, the instrument consists of two reflective surfaces separated by a distance d. When a light beam enters the space between the surfaces, a small portion of the light is transmitted every time it reaches the second surface, while the rest of the light re-

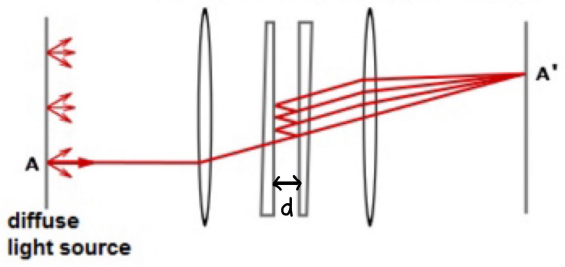

Figure 3: The set up of a Fabry-Pérot interferometer [5]. The distance d shows the distance between the two mirrors.

flects back. The distance d between the mirrors cause a path length difference between the subsequent and transmitted waves. The multiple transmitted light beams are focused through a lens onto a screen where they interfere producing a pattern of bright and dark bands. This pattern in known as an airy disk. Complete constructive interference result in the brightest bands, while partial constructive interference results in the darker bands [6]. In solar physics, the Fabry-Pérot interferometer is among other things, used to measure Doppler shift by studying the interference patterns for specific wavelengths [2].

C. Examples of solar observation instruments

The solar telescope, Swedish 1-m Solar Telescope which was used to gather the observational data used in this report has two instruments using a Fabry-Perot interferometer. These two instruments are called CRISP and CROMIS [2]. On NASA's Hubble Space Telescope we find the STIS (Space Telescope Imaging Spectrograph) which is a slit-spectrograph used for separating light into different wavelengths [7].

D. Comparison of slit-spectrograph and Fabry-Pérot interferometer

Both the slit-spectrograph and the Fabry-Pérot interferometer is used for spectroscopy. One difference is that the slit-spectrograph measures one spatial dimension X and the wavelength dimension λ for a given time as shown in figure 4. To obtain the second spatial dimension, one needs to move the slit across the solar disk resulting in the spectra at the other spatial dimension Y being measured at different times. This process is known as scanning [3]. The Fabry-Pérot interferometer, on the other hand, measures two spatial dimensions (X, Y) at the same time for a given wavelength as shown in figure 5. A similarity between the two instruments is that they both use interference patterns to observe certain wavelengths [2]. Another difference between the two instruments is that the Fabry-Pérot interferometer produce interference patterns with

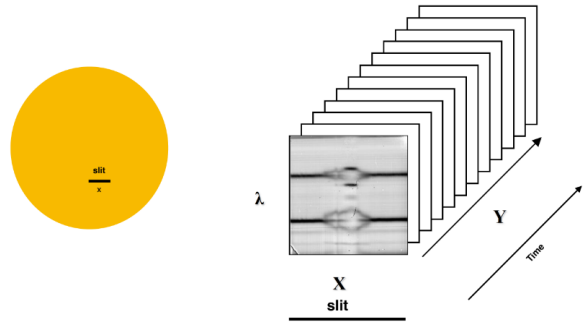

Figure 4: The dimensions measured by a slit-spectrograph [3].

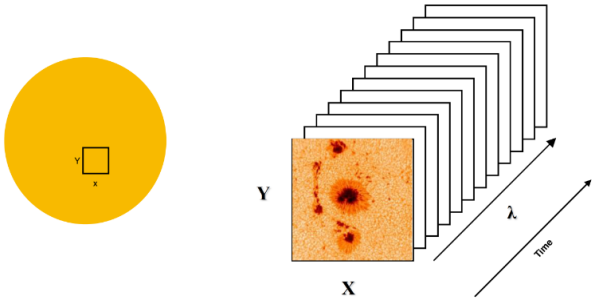

Figure 5: The dimensions measured by a Fabry-Pérot interferometer [3]

high spectral resolution only by changing the distance d between the mirrors. To increase the spectral resolution of a slit-spectrograph, one would need to increase the number of slits in the grating which is more cumbersome than just adjusting the mirrors in the Fabry-Pérot interferometer. The Fabry-Pérot interferometer also uses different filters that allow light of only a specific wavelength to pass through, making it easier to study certain wavelengths of interest. Filters like this are not commonly used for slit-spectrographs [2].

E. Granulation pattern

The photosphere is the visible surface layer of the Sun. This layer consists almost entirely of granules except for some few areas where we have Sunspots. The granulation pattern is caused by the convective zone in the layer below. The granules are tops of convective cells which consists of rising hot gas, which makes the center of the granules appear bright. As the gas rises, it spreads out, cools down and starts sinking back to the surface again, creating a darker boundary around the bright centers of the granules. This can be seen in figure 6. These boundaries are called intergranular lanes and are darker and less intense than the centers. Each granule has an average diameter of about 1000 km. The larger the granule,

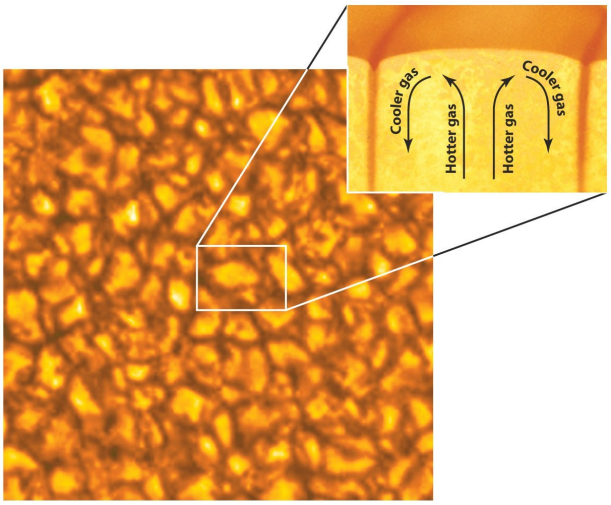

Figure 6: Granulation pattern in the solar photosphere. In each granule cell, hot gas is rising in the center, cools down and sinks back down due to convection [9].

the longer lifetime it has. A granule on average last about 8-20 minutes before it dissipates. New granules are born either as a result of one large granule splitting, or as a result of two granules merging [8].

F. Doppler velocity

The Doppler effect is the change in wavelength caused by relative motion between the source and an observer. If the light source is moving towards the observer (who is standing still) the wavelength of the waves appear shorter, which is what we call blueshift. If the source is moving away from the observer, the wavelength appear longer causing a redshift. The velocity at which the source is moving relative to the observer is the Doppler velocity, and can be calculated using equation 1

$$v = c\frac{\Delta\lambda}{\lambda_{em}} = c\frac{\lambda_{obs} - \lambda_{em}}{\lambda_{em}} \tag{1}$$

where λ_{obs} is the wavelength the observer is measuring, λ_{em} is the wavelength emitted by the source and c is the speed of light [2].

For a given spectral window, i.e. a given absorption line λ_{em}, the Doppler velocity of different parts of the granulation pattern in the solar photosphere can be calculated by analyzing spectra of a given line of sight and equation 1. From the spectra we find λ_{obs}. Having values for the Doppler velocity in different parts of the granulation pattern, we can determine the motion of the surface mass. When gas rises in the middle of a granule, we will get a blueshift as the gas is moving towards us.

III. METHODS

The observational data was taken by the CRISP instrument which uses a Fabry-Pérot interferometer. The observation is of a rectangular field of view centered at $(x, y) = (-421, -274)$ arcsec. This corresponds to a position on the Sun about half-way from the center of the solar disc $(x, y) = (0, 0)$ and the solar limb. The observational data was stored in two files named `idata_square.npy` and `spect_pos.npy`. The first file, `idata_square.npy`, has dimensions $(y, x, \lambda_i) = (550, 750, 8)$ containing intensity as a function of wavelength λ. The spatial units are pixels and λ_i is 8 wavelength locations. The numerical values at each index is the intensity. The second file `spect_pos.npy` contains the wavelength value in Ångstrom for the 8 wavelength indices λ_i in `idata_square.npy` [10].

To calculate the physical size of the photospheric field of view, we use that the spatial dimension of the data is $(x, y) = (550, 750)$ pixels, the spatial resolution of the data is 0.058 arcsec per pixel and that 1 arcsec corresponds to 740 km on the photosphere [10]. First we turn the spatial dimension from pixels to arcsec, then from arcsec to kilometers. Lastly we multiply the two spatial dimensions x and y to get the physical size in km^2.

To study the absorption spectra of the Sun, we choose four points in our field of view and plot the spectra. The four points we choose have pixel locations as shown in table I. From our two datasets we retrieve the intensity observed for all 8 wavelengths from `idata_square.npy` and plot them against the wavelength value given in Å from `spect_pos.npy`.

Point	**Pixel location** (x, y) **[pixels]**
A	(49, 197)
B	(238, 443)
C	(397, 213)
D	(466, 52)

Table I: The spectral positions of the four points that we look further into in our field of view [10].

We want to compare each of the four spectra to the spectra averaged over the whole region. The averaged spectra is calculated by first taking the average of all the intensity data in x-direction and then taking the average over the already calculated average, but now in y-direction. That leaves us with 8 averaged intensity values for each of the wavelengths. To easier compare the average intensity to the spectra for each point, we add the average spectra graph in the four previous spectra.

Wanting to further study the intensity from the Sun we plot an intensity image using the intensity data from `idata_square.npy`. We do this for the wavelength location $\lambda_i = 4$. We give each pixel a color corresponding to its intensity value so that we get a coloured image representation of the intensity in each pixel position. To make the visualization easier to read and compare to our knowledge about granulations, we chose a colorbar that goes from the color white for max intensity, then to yellow, red and black for lower intensities. This is easier to read since the middle of granulations appear bright as a result of their high intensity, while the intergranular lanes appear darker since they are less intense. We mark the points A, B, C and D in the image as white circles.

To look more in detail at the granulation pattern we plot the intensity image for a sub field of view. This is done by slicing out a small grid from the whole intensity dataset. The sub field of view has a hight of 100 pixels and width of 150 pixels and the coordinates of the lower left corner is $(x, y) = (525, 325)$. Before slicing the data, we mark the border of the sub field of view in the full field of view intensity image. Then we slice the dataset `idata_square.npy` and plot the intensity image for the sub FOV in the same way we did for the full field of view.

Since absorption lines have a close resemblance to a Gaussian function, we fit a Gaussian to the spectral data for each of the four points A, B, C and D using the Gaussian function defined as

$$g(x, \mathbf{P}) = ae^{-\frac{(x-b)^2}{2c^2}} + \mathbf{P} \tag{2}$$

where $\mathbf{P} = (a, b, c, d)$ is the parameters of the function [10]. To find the most optimal parameters we first estimate each of them, then use the non-linear least squares method `scipy.optimize.curve_fit()` to calculate the best fit. To estimate a, which is the amplitude of the Gaussian, and therefore the difference of the peak value and the baseline, we calculate the difference between the intensity with highest and lowest value. To estimate b which is the mean of the Gaussian, we find the wavelength at which we have the peak of the Gaussian. The parameter c which is the standard deviation was estimated to a constant by looking at the different spectra. Lastly we estimate d which is the y-value of the baseline by finding the max intensity value in the spectra.

We insert the optimized parameters of $\mathbf{P}$ that we got from the least squares method into equation 2 and plot the function against a new defined, evenly spaced wavelength-interval from the lowest wavelength value in the spectrum to the highest. This we do for each of the four points.

We know that the wavelength window we are studying is centered around Fe I at 6173 Å [10]. Therefore we try to estimate the central wavelength of the absorption line to see if it is the same. This we do by first fitting a Gaussian to the average spectra which we calculated earlier. Then we use the optimized parameter b from the Gaussian function as the central wavelength because this is the wavelength at which the average spectra has its peak. To find the error in the estimated wavelength we retrieve the square root of diagonal value of the covariance matrix returned by `scipy.optimize.curve_fit()` which corresponds to the standard deviation error of the parameter b and therefore also the error in the central wavelength.

To see which parts of the solar surface in our field of view is moving towards us, and which parts are retracting we calculate the Doppler velocity. First we calculate the Doppler velocity for the four points A, B, C and D using equation 1. The emitted wavelength λ_{em} is the central wavelength of 6173 Å and λ_{obs} is the wavelength in the peak of the Gaussian which we get from the optimized parameter b.

To calculate the error of the doppler velocity Δv, we use the error propagation formula and get the expression in equation 3.

$$\Delta v = \sqrt{\left(\frac{\partial v}{\partial \lambda_{obs}} \Delta \lambda_{obs}\right)^2} = \frac{c}{\lambda_{em}} \Delta \lambda_{obs} \tag{3}$$

To find the error $\Delta \lambda_{obs}$ we again retrieve the square root of the diagonal element of the covariance matrix that we get from `scipy.optimize.curve_fit()` which gives us the standard deviation error in b. Since $\lambda_{obs} = b$, the error in b is equal to $\Delta \lambda_{obs}$.

Now we create a Doppler map by calculating the Doppler velocity in every point of our field of view. We do this the same way that we did for the four points and let each Doppler velocity correspond to a color ranging from red (positive velocity) and blue (negative velocity) in the same way that we did for the intensity image. We also slice out the calculated Doppler velocities for the sub field of view and plot the Doppler map for this separately.

The last thing we want to investigate is how the intensity compares to the doppler velocity. We therefore make a scatterplot with all the intensity values on the y-axis, and all the Doppler velocity values on the x-axis.

IV. RESULTS

The physical size of the photospheric field of view was calculated to a size of $759\,877\,140\,\mathrm{km}^2$ using these values:

$$(550, 750)\,\text{pixels} \cdot 0.058'' = (31.9, 43.5)''$$
$$(31.9, 43.5)'' \cdot 740\,\mathrm{km} = (23\,606, 32\,190)\,\mathrm{km}$$
$$(23\,606 \cdot 32\,190)\,\mathrm{km} = 759\,877\,140\,\mathrm{km}^2$$

In figure 13 (placed in appendix due to size), we see the absorption spectra for the four points A, B, C and D

which have pixel locations as listed in table I. The four absorption spectra show the intensity data as a function of the wavelength value, the Gaussian fit to the spectra and a comparison to the average intensity curve.

In figure 7 we see the intensity image plotted using data from `idata_square.npy` for wavelength $\lambda_i = 4$.

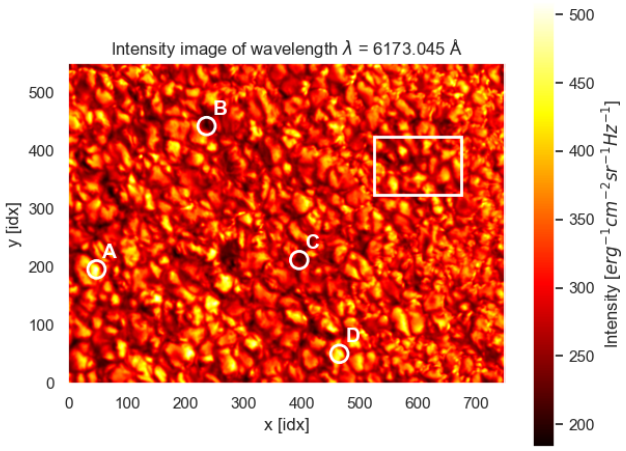

Figure 7: The intensity image for our whole field of view plotted using data from `idata_square.npy` for $\lambda_i = 4$. The points A, B, C and D with pixel locations shown in table I are marked with white circles in the plot. The white square shows our sub field of view shown in figure 8.

The intensity image of our sub field of view is shown in figure 8. This intensity image is also plotted for $\lambda_i = 4$.

The value of the central wavelength was estimated to 6173.004 ± 0.002 Å from fitting a Gaussian to the average spectra. This value is marked in figure 9.
The Doppler velocity of the four points A, B, C and D was calculated to the values shown in table II using equation 1.

Point	Doppler velocity [m/s]
A	-3547 ± 128
B	1803 ± 59
C	1637 ± 74
D	-2555 ± 129

Table II: The calculated Doppler values for points A, B, C and D using equation 1. The errors were calculated using equation 3.

Figure 10 shows the Doppler map of our full field of view using equation 1 for every pixel location in our field of view. The red areas correspond to a redshift, and the blue areas correspond to a blueshift.

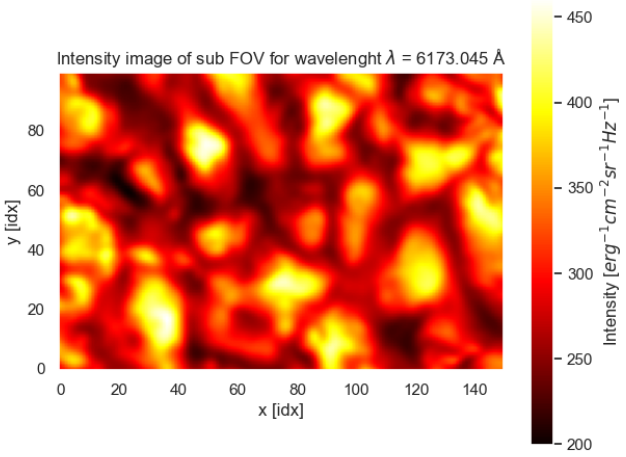

Figure 8: The intensity image of our sub field of view plotted by slicing out the white rectangle in figure 7. The intensity image is plotted for $\lambda_i = 4$.

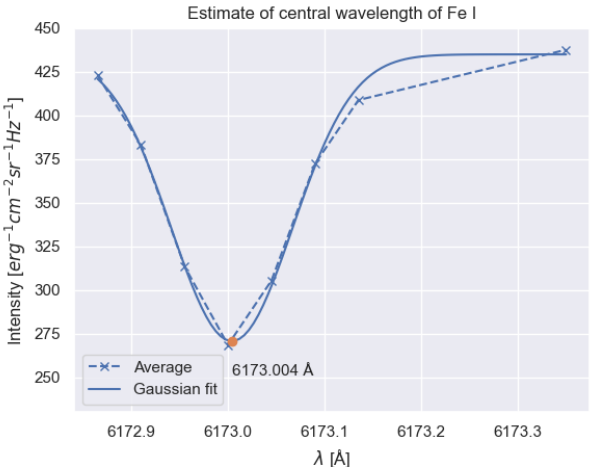

Figure 9: The dashed graph shows the average intensity plotted against the wavelength values in Å from `spect_pos.npy`. The blue, whole line shows the Gaussian fit to the average spectra and the orange dot shows the peak of the Gaussian which is what we estimate as the central wavelength.

In figure 11 we see the Doppler map for our sub field of view, plotted by slicing the Doppler velocities from the full field of view in the sub field of view location.

To compare the intensity and the Doppler velocity we plotted the two datasets against each other in figure 12. Due to the large amount of datapoints, the size of each point was set to be very small to easier see the trends. This plot is for the wavelength location $\lambda_i = 4$.

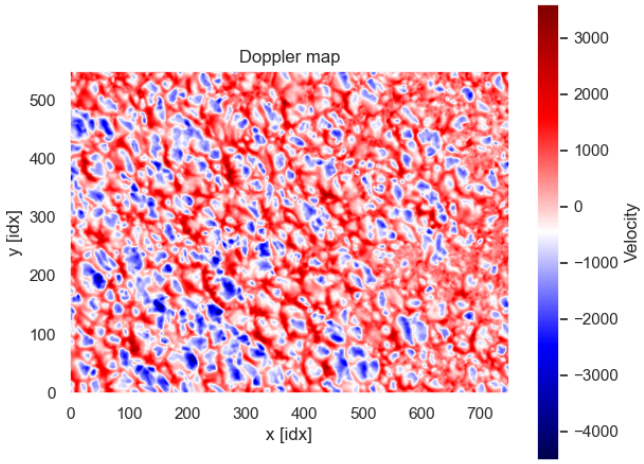

Figure 10: The Doppler map for our full field of view. The velocity goes from positive to negative where red is positive velocity and blue is negative velocity.

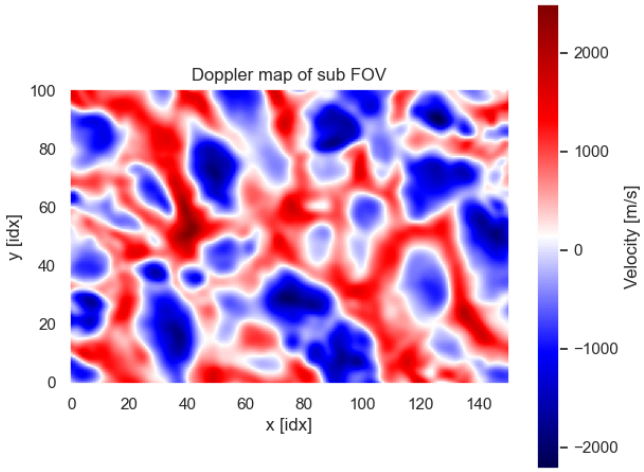

Figure 11: The Doppler map for our sub field of view. This is from the same grid location and size as the sub field of view in the intensity image was.

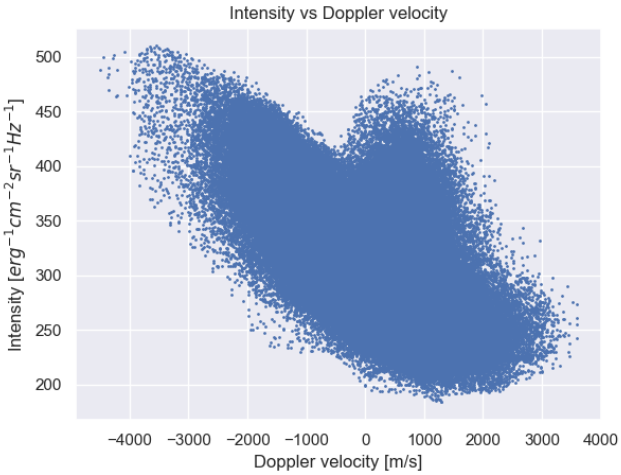

Figure 12: Scatterplot of the intensity vs the Doppler velocity. Each dot in the figure represent a datapoint. This was plotted for $\lambda_i = 4$.

V. DISCUSSION

A. Spectra analysis

We see that the spectra for point A and D found in figure 13 are similar to each other and their peaks looks to be shifted more to the left of the average spectra and the central wavelength of $\lambda = 6173$ Å. A shift to the left is a shift towards shorter wavelength which indicates that these two spectra are blueshifted. The two other spectra for point B and C are shifted a bit to the right of the average spectra and the central wavelength, towards longer wavelengths indicating a redshift. If we look at the four points in the intensity image in figure 7, we see that point A and D are placed in the center of two granules confirming why the spectra is blueshifted. The hot gas rising in the middle of the granules appear to be moving towards us resulting in a blueshift from the Doppler effect and the wavelength appears shorter. In the same figure, figure 7, we see that point B and C are placed on two intergranular lanes explaining their redshift since the gas is moving back towards the surface of the Sun, meaning away from us (the observer).

B. Intensity image

The intensity images are shown in figure 7 for the full field of view, and figure 8 for the sub field of view. We study the sub field of view image first, as this shows the granulation pattern more clearly. As explained in section II E, the granulation pattern we see is due to convection in the convective zone. In figure 8 we observe this granulation pattern. The yellow parts we see are the centers of the granules which have a high intensity caused by the hot gas rising. The red/black outlines of the yellow parts are the intergranular lanes which appear darker with lower intensity due to the gas cooling and falling back down again. If we look at the intensity image for the whole field of view, we see that the two points A and D are located at the center of two granules where hot gas is rising, while the points B and C are placed on darker parts where the gas is cooling.

C. Doppler velocities

The calculated Doppler velocities for points A, B, C and D are shown in table II. From equation 1, we see that if $\lambda_{obs} > \lambda_{em}$ the Doppler velocity becomes positive. If the inequality is true, it means that when the Doppler velocity is positive, we are observing light with longer wavelengths than the source emits and the light is redshifted. From this we can see that because the Doppler velocity for points B and C are positive, the light from these locations are redshifted (as we also saw from the intensity image and spectra). The points A and D have negative Doppler velocities, meaning a blueshift.

The errors we calculated using equation 3 are quite big. The only contributor to the calculated error is the error in the observed wavelength, λ_{obs}, that we get from the covariance matrix calculated by `scipy.optimize.curve_fit()`. It is worth noting that we estimate λ_{obs} from the spectra, which only consist of 8 observation points. If we had more datapoints the Gaussian fit would be better resulting in the estimation of λ_{obs} from the peak of the Gaussian fit being more precise. Another contributing factor could be the rotation of the Sun that we are not taking into account in our calculations. The rotation could lead to a shift in velocity, but we need to calculate how big this contribution would be to determine if this is affecting the error in Doppler velocity for the four points.

D. Doppler map

By calculating the Doppler velocity for each pixel location in the field of view we could make the Doppler maps shown in figure 10 and 11. As we did for the intensity image, we choose to look at the sub field of view first as it is easier to see the pattern. We see that the pattern resembles the pattern we saw in the intensity image, figure 8, only this time in red and blue. The blue color is for negative Doppler velocities corresponding to blueshift and red for redshift. If we compare the two images we see that the granule centers with high intensity correspond to the blue parts of the Doppler map which makes sense since we have seen that the hot air rising from the granule centers result in a blueshift.

E. Central wavelength estimation

When estimating the central wavelength of the Fe I absorption line we got the value $\lambda = 6173.004 \pm 0.002$ Å, which is a good estimate when we know that the actual value was $\lambda = 6173$ Å. We see that this error is much smaller than the error we got for the Doppler velocities in table II. The reason for this might be that we use the average spectra for finding the central wavelength, and not just the 8 points in one spectra, resulting in more observational points than we have for a single spectra.

F. Intensity vs Doppler velocity

We plotted the intensity vs Doppler velocities in figure 12. This plot changes for different wavelength locations, and since we chose $\lambda_i = 4$ for the intensity plot, we use that value here too. We see that for the Doppler velocities with a high negative value has the highest intensity, while the positive Doppler velocities in general have a lower intensity except for the increasing intensity for Doppler velocities around $v = 1000$ m/s. If we compare with the Doppler velocities in table II, we see that points A and D, which have a high negative value, also have a high intensity as they are located in the center of granules. Points B and C which have a Doppler velocity with positive value have lower intensities being located in the intergranular lanes.

VI. CONCLUSION

Analyzing the observational data obtained by the SST we first found the spectra for four different points on the surface with pixel locations given in table I. Fitting a Gaussian function to the spectra in figure 13 we were able to calculate the Doppler velocity in those four points using equation 1. The error in these velocities was quite big, probably because of too few datapoints for each spectra. The Doppler velocity was also calculated for each pixel location in our field of view which we used to make the Doppler map in figure 10. Comparing the sub field of view Doppler map in figure 11 to the intensity image in figure 8 we could see that the granule centers corresponded to the blue parts in the Doppler map representing blueshift since this is where hot gas rises and moves towards us making the wavelengths appear shorter. We also saw that the red parts of the Doppler map corresponded to the intergranular lanes in the intensity image where the gas is cooler and moving away from us, making the light redshifted.

To improve our model we could obtain more datapoints for each spectra and include the rotation of the Sun for our Doppler velocity calculations.

[1] A. T. N. Facility, "Obtaining astronomical spectra - spectrographs," .
[2] R. Joshi, "Fabry-pérot interferometer (fpi)," University Lecture (2023).
[3] R. Joshi, "Principle of grating spectrograph," University Lecture (2023).
[4] O. College, "Multiple slit diffraction," .
[5] S. aurantiaca, "Fabry perot interferometer," .
[6] "Fabry perot interferometer," .
[7] R. Garner, "Observatory - instruments — space telescope imaging spectrograph," (2023).
[8] E. Priest, *Magnetohydrodynamics of the Sun* (Cambridge University Press, 2014).
[9] C. for Science Education, "Inside the sun," .
[10] R. Joshi and I. J. S. Poquet, "Ast2210: Assignment 1 - solar observation," University assignment (2023).

Appendix A: Spectra with Gaussian fitted curves compared to average spectra

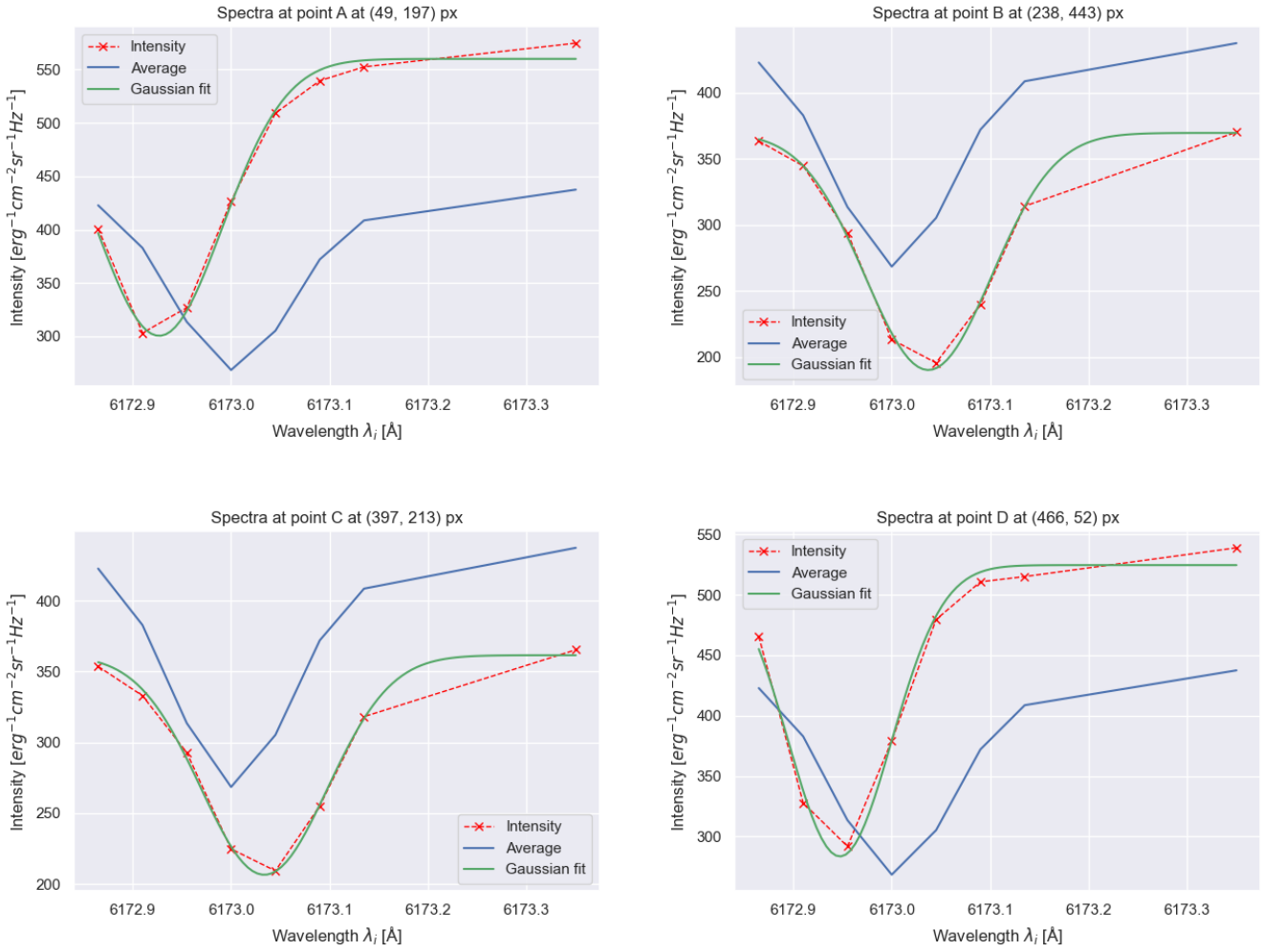

Figure 13: All the spectra plots above show the intensity data from `idata_square.npy` plotted against the wavelength value from `spect_pos.npy` in red. The Gaussian fit of each spectra is also included in green. For comparison we included the average spectra in each plot in blue. The top left figure shows the absorption spectra for point A, the top right figure shows the absorption spectra for point B, the bottom left figure shows the spectra for point C and the bottom right figure shows the spectra for point D.